FISEVIER

#### Contents lists available at ScienceDirect

# Marine Chemistry

journal homepage: www.elsevier.com/locate/marchem



# Observations and idealized modelling of microplastic transport in estuaries: The exemplary case of an upwelling system (Ría de Vigo, NW Spain)



Manuel Díez-Minguito<sup>a,b</sup>, María Bermúdez<sup>a,b,\*</sup>, Jesús Gago<sup>c</sup>, Olga Carretero<sup>c,d</sup>, Lucía Viñas<sup>c</sup>

- <sup>a</sup> Andalusian Institute for Earth System Research (IISTA-CEAMA), 18006 Granada, Spain
- <sup>b</sup> Dept. Structural Mechanics and Hydraulics Engineering, University of Granada, 18071 Granada, Spain
- c Instituto Español de Oceanografía (IEO), Subida a Radio Faro, 50-52, 36390 Vigo, Spain
- <sup>d</sup> Campus do Mar, Facultad de Ciencias del Mar, Universidad de Vigo, 36310 Vigo, Spain.

#### ARTICLE INFO

# Keywords: Microplastics Estuarine dynamics Ría de Vigo Trapping Sampling Mathematical models Vertical distribution Suspended particulate matter

#### ABSTRACT

Microplastics (MPs) pollution in marine environments has received considerable attention over the past two decades due to the increased awareness of its potential risks to ecosystems. Numerical simulations can be used to provide estimates of MPs fate and distribution, but so far this approach has been largely applied to the open ocean. In this work, the distribution patterns of MPs in a prototype coastal upwelling environment (Ría de Vigo estuary, Spain) is investigated using a combined approach of field data and modelling. Water and sediment samples were collected at different locations along the Ría during both upwelling and downwelling conditions. Experiments using an idealized 2D-vertical model were conducted to explain the observed MP distribution and elucidate the relative importance of river discharge, wind-driven and density-driven circulation. Microplastics were found at all stations in all samples. The largest observed fraction of MPs corresponded to fibres followed by plastic paint sheets and fragments. The trapping or flushing of MPs was mainly controlled by the wind forcing, whose effects on the circulation normally exceeds those of the density-driven and river flows. During upwelling conditions, more MP items were collected near the surface at the outer half of the estuary than during downwelling. The seaward near-surface circulation induced by the wind and density gradient jointly contributed to flushing out floating MPs. Near the bottom, the landward wind-induced and gravitational circulation formed estuarine MP maxima (EMPM) inside the estuary. Pellets, fragments, and films were more efficiently trapped than fibres, as their EMPM were located more upstream. The results suggested that downwelling-favourable winds caused an overall landward (seaward) displacement of the distribution of floating (sinking) MPs. Modelling results indicate that winds dominate the circulation in the outer part of the estuary, whereas near the head the gravitational circulation takes over the control of the net flow. The particular location of the EMPM appears to be controlled by the competition of density-driven and wind-driven flows.

# 1. Introduction

The large-scale production of plastics began around 1950. The versatility of plastics combined with their low cost, the global population growth and the increase in widespread consumption habits have led to an exponential increase in the demand of this material worldwide. According to Geyer et al. (2017), 6300 million Mt of plastic waste has been produced between 1950 and 2015, of which only 9% has been recycled, 12% incinerated, and the other 79% is accumulated in landfills or the environment.

Seas and oceans are the final destinations of a large fraction of the plastic waste released into nature since they are at the lowest level in the drainage direction of inland waters. According to Jambeck et al.

(2015), between 4.8 and 12.7 million Mt of plastic enters the marine environment yearly. The proliferation within the marine environment of plastic particles below 5 mm, the so-called microplastics (MPs), is of particular concern. Primary MPs (i.e., purposefully manufactured to be small) include micro-beads in cosmetic preparations, scrubbers used in air-blasting technology, microspheres used as carriers of medications into body tissues or virgin plastic production pellets (Cole et al., 2011). However, the vast majority of MPs in the oceans is believed to originate from larger plastic items that fragment (secondary MPs). This weathering process occurs particularly rapidly in the beach environment (Andrady, 2011). Due to the diversity of origins and polymer compositions, the physical characteristics of MPs span a wide range of shapes (e.g. spheres, fibre, film, irregular, etc.) and densities (from 16 to

<sup>\*</sup> Corresponding author at: Avda. del Mediterráneo s/n. Edificio CEAMA, 18006 Granada, Spain. E-mail address: mariabermudez@ugr.es (M. Bermúdez).

 $2200 \, \text{kg m}^{-3}$  according to Nizzetto et al. (2016)), which results in very different behaviour in the aquatic environment.

Microplastic pollution in marine environments is currently receiving much attention due to the increased awareness of its potential risks to human health and wildlife. MPs may physically harm marine organisms once ingested, by internal abrasion and ulceration, as well as obstruction and blockage of the digestive system (Wright et al., 2013). These physical effects may be enhanced by toxic responses due to chemicals contained within the plastic itself (e.g. additives) or pollutants adsorbed from the surrounding environment (e.g. persistent organic pollutants and metals) (Mato et al., 2001; Holmes et al., 2014).

This growing concern has led to numerous studies on the abundance and distribution of MPs in the marine environment, most of which focused on the open ocean (Cózar et al., 2014; Onink et al., 2019). The large-scale oceanic gyres have been extensively studied (e.g. Maximenko et al., 2012; Lebreton et al., 2012). However, much of the plastic debris that makes its way out to sea comes from land-based sources, via rivers and their estuaries. Based on global estimations (e.g. Kershaw, 2016), land-based sources (such as wastewater treatment plants, coastal landfills, etc.) contribute to around 80% of marine litter worldwide. Sea-based sources, derived from activities such as fishing and maritime transport, represent the remaining 20%. Related to the land based sources, it is also important to mention that around half of the world's population lives in coastal areas, within ~60km from the shoreline (Kershaw, 2016). In consequence, emissions directly associated with anthropogenic activities such as, for example, those from ports are very important as a direct source.

Transitional areas between the land and the sea thus constitute a key zone to monitor plastic emissions to the world's ocean and to prevent plastic waste from reaching the ocean. The study of fluxes, accumulation zones, and degradation of MPs in transitional waters is a very promising research area, which has received little attention so far (Windsor et al., 2019; Simon-Sánchez et al., 2019). As a result, the role of estuaries on the flushing or trapping of MPs from land to sea remains largely unknown. Estuaries act as accumulation areas for sediments, nutrients and pollutants (Eisma, 2012), which suggests that they can be not only a source of MPs pollution for coastal waters but also a potential sink of land-based MPs sources. Some recent studies have evaluated the input of plastic pollution entering the sea from river basins (Lebreton et al., 2017). However, these studies do not consider the transition zone from the river mouth to the open ocean, which could reduce the amount of MPs ultimately transported to the sea. An observation supporting this view has been made in the recent study by Xiong et al. (2019), which shows that a considerable amount of MPs generated in large river catchments are not transported to the sea due to the existence of traps for MPs along the river-estuary continuum. As a consequence, past modelling estimates of MPs fluxes may contain biases which can only be addressed by gaining a deeper understanding of the transfer pathways from rivers to the open sea, and identifying the hotspots (viz. Estuarine MP Maxima, EMPM) for MPs concentration in estuaries and their meteorological and oceanographic drivers.

Intending to fill this gap, this research addresses the following objectives:

- To quantify concentration, properties, and distribution of MPs in a prototype coastal upwelling system,
- To unravel the relative influence of the river discharge, the winddriven, and the density-driven circulation on the MPs distribution, and
- 3. To identify the trapping conditions of MPs in the estuary, both at the bottom and near the surface.

These objectives were addressed employing a combined approach of observations and modelling in the Ría de Vigo, which is a prototype estuarine system subject to seasonal variations induced by the large-scale wind patterns driving upwelling and downwelling. To address the

first research objective, water and sediment samples at the near-surface and bottom, respectively, were collected at different locations along the Ría under different meteorological and oceanographic conditions. Concentration and distribution of MPs in the Ría, as well as shapes, type of plastic, and color, were determined. To address the second and third questions, an idealized model (2D-vertical) was implemented to evaluate the distribution of MPs, and gain basic knowledge into the transport mechanisms that control their along-estuary and vertical distribution. The approach adopted here to determine concentrations of both sinking and floating MPs in the Ría de Vigo builds upon that devised by Talke et al. (2009b), which succeeded in explaining the main features of the circulation and suspended sediment patterns in estuaries. Model output was compared with field observations in the Ría de Vigo. This approach allowed the quantification of the role of the circulation induced by various factors (river discharge, wind-driven and density-driven circulation) on the distribution of MPs in the Ría de

The manuscript is organized as follows. Section 2 describes the study area, the sampling and MP processing methods, and the idealized model approach. Section 3 presents the analyses of the observations and the model results on the circulation and the MPs distribution in the Ría de Vigo. The implications derived from the analysis of observations and modelling results are discussed in Section 4. Finally, Section 5 summarizes the main conclusions of this study.

#### 2. Materials & methods

# 2.1. Ría de Vigo

The Ría de Vigo (Fig. 1) is located in the NW coast of the Iberian Peninsula, which is part of a coastal upwelling ecosystem at the eastern North Atlantic. The middle and inner Ría comprises over  $L=16\,\mathrm{km}$  from its mouth to the head at Rande Strait. This part of the Ría is strongly convergent, i.e., it shows widths that vary from 11 km near the mouth to 0.7 km at the head, and lateral circulation is usually weaker than longitudinal circulation due to the narrowness of the basin (e.g. Barton et al., 2015). Along-channel mean depth is about 30 m, with its maximum near the mouth (40 m). Tides are mesotidal (lower than 4.5 m), and the large depths in the Ría often cause a partially-mixed water column structure.

The climate in the Ría de Vigo is warm-summer Mediterranean, often cooled by ocean currents, according to Köppen classification. Shelf winds exhibit marked seasonal variations in magnitude and duration associated to the NE Atlantic climate. The upwelling and downwelling-favourable winds are important drivers of the circulation patterns in the Ría de Vigo (e.g. McClain et al., 1986). Upwelling conditions prevail from March-April to September-October favoured by northern winds (e.g. Gilcoto et al., 2007). The Ría de Vigo exhibits along its central and inner parts a positive estuarine circulation, i.e., fresher outflows near the surface and inflow of denser seawater near the bottom (Taboada et al., 1998). This situation coincides with periods of relatively low precipitations, which yield low river flows from the Oitaven and Verdugo rivers (Fig. 1). These rivers, both located at the estuary head, supply most of the freshwater runoff to the Ría. The monthly-averaged discharges of the Oitaven and Verdugo rivers range approximately between 1 m<sup>3</sup>s<sup>-1</sup> and 7 m<sup>3</sup>s<sup>-1</sup>, and between 0.5 m<sup>3</sup>s<sup>-1</sup> and 6 m<sup>3</sup>s<sup>-1</sup>, respectively, during those upwelling periods. Secondary freshwater sources are the Lagares and Alvedosa rivers.

The rest of the year downwelling-favourable winds prevail and freshwater discharges increase (wet season). Monthly-averaged discharges from Oitaven and Verdugo attain values as high as  $\sim 27~{\rm m}^3{\rm s}^{-1}$  and  $\sim 18~{\rm m}^3{\rm s}^{-1}$ , respectively. During those conditions, a wind-induced reverse or negative estuarine circulation may arise in the Ría, thereby showing landward flow near the surface and return flow near the bottom (Villacieros-Robineau et al., 2013). During high river discharge and downwelling conditions, the buoyant plume of the Miño River may

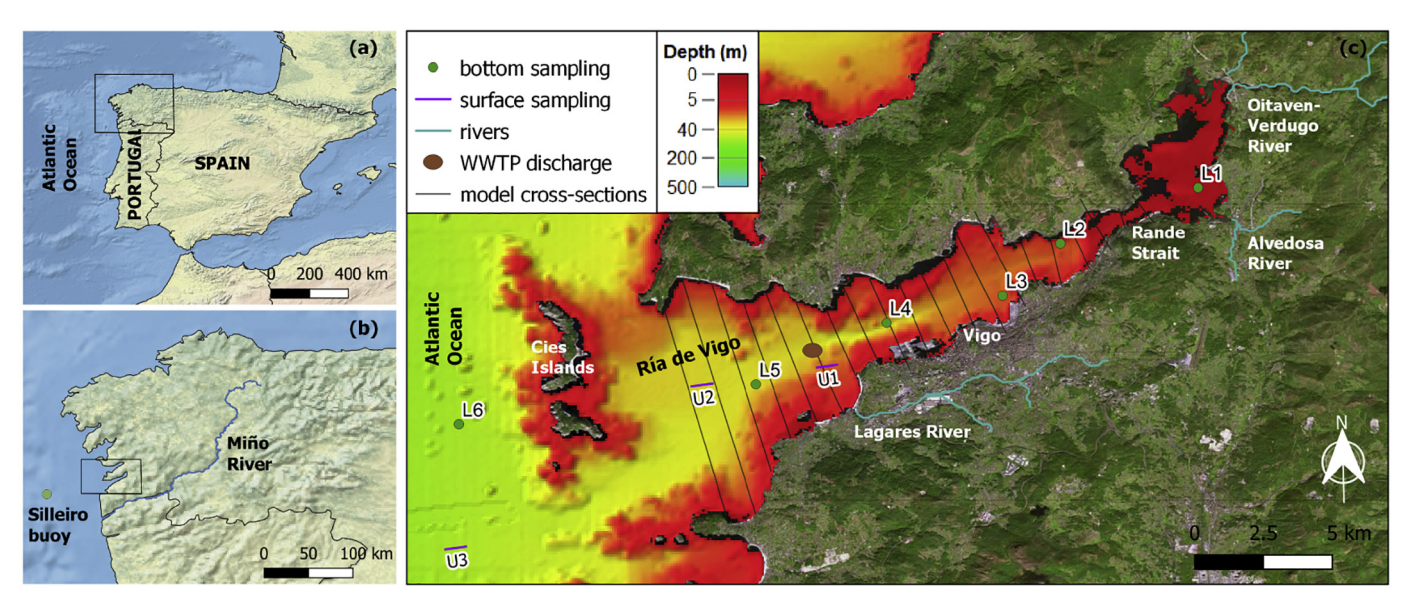


Fig. 1. Location of the study area in the Iberian Peninsula (panel a) and in the Atlantic margin of Galicia (panel b); Bathymetric contour map overlaid onto an aerial image of the Ría de Vigo estuary (panel c), showing: the main rivers flowing into the estuary, the location of Vigo city and Cíes Islands (National Park), the Vigo wastewater treatment plant (WWTP) discharge point (filled brown ellipse), the cross-sections used to set up the numerical model, and the position of the sampling stations for surface and bottom waters (U1 to U3, and L1 to L6, respectively). (For interpretation of the references to color in this figure legend, the reader is referred to the web version of this article.)

influence the Ría de Vigo circulation. The Miño River is the most important river flowing near this coastal system and periodically influences the Ría de Vigo waters. Monthly-averaged discharges from the Miño approximately range between  $100\,\mathrm{m}^3\mathrm{s}^{-1}$  in summer and  $800\,\mathrm{m}^3\mathrm{s}^{-1}$  in winter (Sousa et al., 2014). The Miño plume may freshen the waters at the mouth of the Ría de Vigo, thereby promoting a density-driven negative circulation inside. These events, which have recently received ample attention (Sousa et al., 2014; Des et al., 2019), are characterized by the landward intrusion of fresher coastal waters at the surface and a compensating seaward flow near the bottom.

Regarding its environmental status, the Ría de Vigo is subjected to strong human impacts (Fernández et al., 2016). At present, the estuary and its immediate surroundings are highly urbanized, hosting ~ 428000 inhabitants clustered in 8 municipalities. The urban pressure is especially important at the central zone of the south seashore, where the city of Vigo is located. The surroundings of the Ría de Vigo are characterized by an important industrial presence which increases the traffic of goods through the Port of Vigo. This is also one of the main fishing ports in the world (e.g. Lopes et al., 2013). Urban and industrial activities carried out in the inner part of the Ría coexist with fishing and mollusk culture (mainly mussels), whose production is favoured by the upwelling conditions. In spite of the generalized impact that the Ría de Vigo sustains, some areas with a low degree of affection still persist that therefore possess high environmental value. Some other studies have focused on the presence of chemical pollutants in the Ría de Vigo (Viñas et al., 2009; Quelle et al., 2011) showing different degrees of pollution.

#### 2.2. Field data

Water and sediment samples were collected in the Ría de Vigo, and subsequently processed in the laboratory, to analyze the MPs properties and distribution. Samples were taken during the flood phase of the tide. Surface seawater samples were collected at stations U1, U2 and U3, which are located at the lower half of the estuary (Fig. 1), during the oceanographic cruise "Radial Vigo" in March and September 2017, using a manta trawl net (3.5 mm in length with a  $300\mu m$  mesh size). The size of the rectangular net opening was  $60 \times 11$  cm. Each sample was obtained at an average speed of 3 knots for 10 min. The volume of water sampled was calculated as the product of the mouth area and the

tow distance. On land the water samples were processed according to the standardised protocol for monitoring microplastics in seawater developed in the JPI-Oceans BASEMAN project (Gago et al., 2018).

Sediment samples were collected during the IMPACTA Cruise in 2015 by means of a Box Corer dredge  $(10.5 \times 17.0 \times 34.5 \text{ cm}^3)$ . Sediments were collected at stations L1-L6 along the Ría de Vigo (Fig. 1). Only the first  $\sim 5$  cm surface bottom sediment were collected to study the plastic pollution. The samples were taken with a stainless-steel slicer and kept in aluminum trays. All samples were frozen at  $-20^{\circ}\text{C}$  for further analysis.

Following the protocol by Frias et al. (2018), sediment samples were defrosted at room temperature. To determine the water content, 3g of sediment were weighed in aluminum cups and introduced in a drying oven at 70°C for 24 h and brought to a constant weight. To extract the MPs, a density separation method was used (e.g. Masura et al., 2015). For each sample, 100 g of sediment were vigorously mixed with 250 mL of a hypersaline solution of NaCl (1.2g/cm³) during 5 min. After 30 min, the heaviest materials settled down and the supernatant was filtered with the Millipore vacuum pump onto the Whatman GF/C filter.

The following methodology was common to the samples collected at U1-U3 and L1-L6 stations, i.e., to bottom and surface samples, respectively. Filters obtained after the laboratory procedure were examined under the stereomicroscope with magnifications  $\times$  0.63 –  $\times$  8 (Leica S8AP0, Leica Microsystems GmbH, Wetzlar, Germany) with image analysis system (Carl Zeiss Axiocam ERc 5s camera and ZEN 2012 software), in order to visually identify and classify plastic particles according to their size, color and type. In order to determine whether a particle is plastic, it should meet the criteria established by Hidalgo-Ruz et al. (2012). The particles found in the filters were photographed and processed with ImageJ program to accurately measure their size and area. The microplastics were classified in six categories according to their type: fibres, filaments, fragments, pellets, rubbers, films and paint sheets following Crawford and Quinn (2016). Fig. 2 shows examples of identified plastics with different shapes, sizes and colours.

Contamination controls were carried out both on the vessel (during sample collection) and in the laboratory (during the extraction and analysis of the filters under the stereomicroscope). They were performed for each sample and consisted of paper filters on Petri dishes exposed to the same possible sources of contamination as the sample

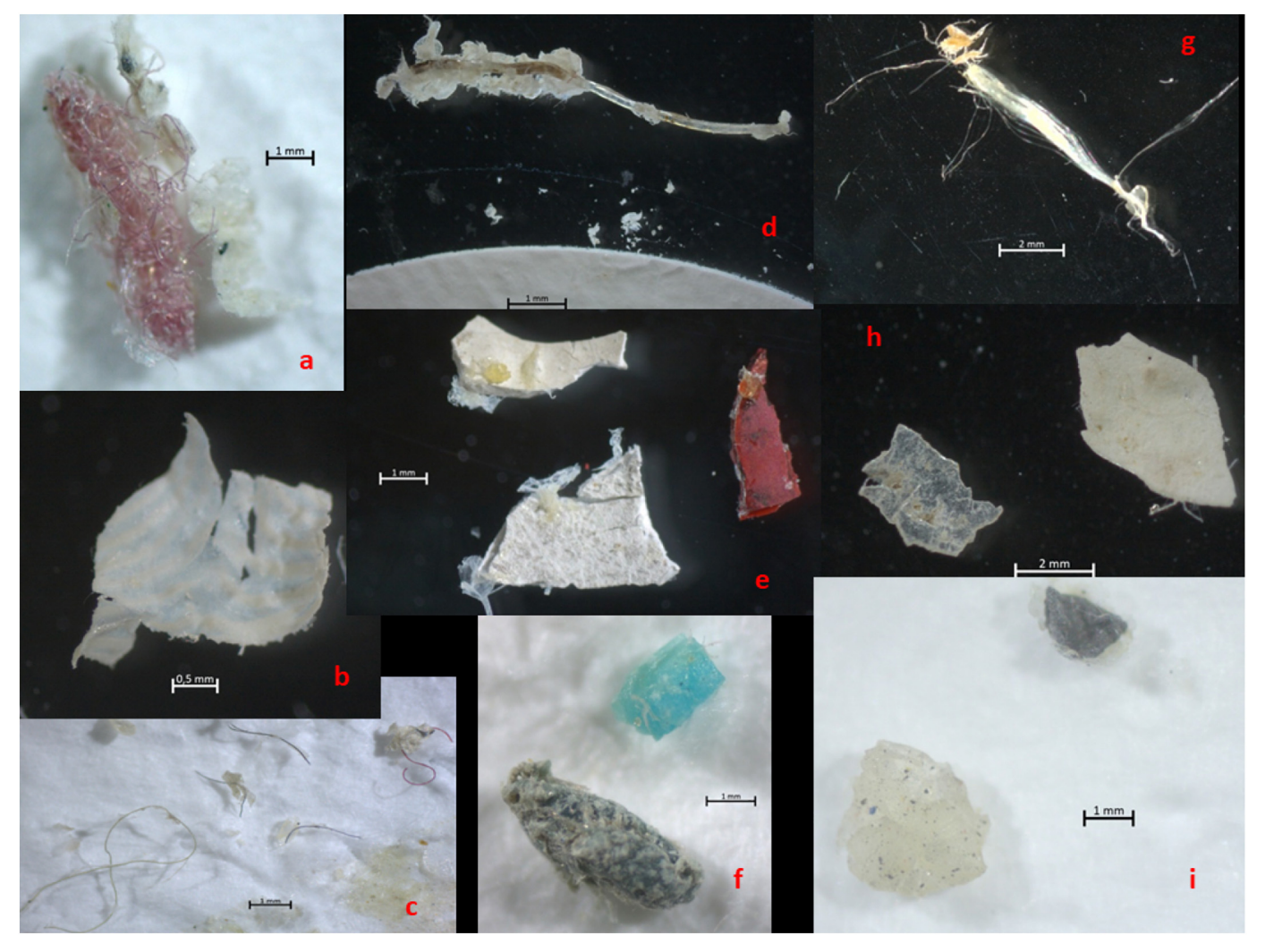


Fig. 2. Plastic samples in the Ría de Vigo: Tangled fibre (a), white film (b), collection of colored fibres (c), filament (d), paint sheets (e), colored fragments (f), filaments degrading into fibres (g), semi-transparent film and white fragment (h), and black and white rubbers (i).

being processed. These controls were analyzed under the stereomicroscope and the plastic particles found were subtracted from the results of the samples. Only 7 fibres were found in the contamination controls on board and laboratory, which were subtracted from the total results. Special care was taken to avoid the contamination during collection, extraction and visual identification of MPs. Only cotton laboratory coats were used, as recommended by Woodall et al. (2015). All lab material used was free of plastics.

Regarding meteorological and oceanographic conditions on the shelf, data were obtained from the Silleiro buoy. Sea level data were obtained from the Vigo2 tidal gauge. These stations are property of the Puertos del Estado government agency (State-owned Spanish Port, Ministry of Public Works) (http://www.puertos.es/es-es/oceanografia/Paginas/portus.aspx). Bathymetric information was extracted from the EMODnet Digital Terrain Model (http://www.emodnet-bathymetry.eu/data-products) at the cross-sections. Mean depths are referenced to the REDMAR datum at Vigo (http://www.puertos.es). Freshwater discharge records for the Verdugo and Oitaven rivers (stations 1585 and 1586, respectively) were collected from the database of the Spanish Centre for Studies and Experimentation in Public Works (http://ceh-flumen64.cedex.es/anuarioaforos/default.asp). Finally, times in this work are provided in mm/dd/yy format.

#### 2.3. Idealized model

# 2.3.1. Basic equations

Subtidal circulation was modelled following Talke et al. (2009b) and de Swart et al. (2009), which succeeded in explaining the main features of the circulation and suspended matter patterns in different estuaries. The module that determines MP concentrations in estuaries is regarded as an adaptation of the model devised by Talke et al. (2009b) for suspended sediment concentration, but also allowing for concentrations of floating litter.

The longitudinal current u(x,z) is determined from an adapted version of the steady, linearized width-averaged shallow water equations (Hansen and Rattray Jr., 1965; Officer, 1976). The model includes the contribution due to the river, density-driven, and wind-induced flows (see Fig. 3). At the bottom, a no-slip condition is imposed. The model is forced at the landward boundary with a given freshwater discharge  $Q_R$  and a horizontal salinity (density) gradient  $\partial S/\partial x$  due to a given along-estuary density distribution, which is prescribed and assumed to be independent of depth. The model assumes a rigid-lid approximation and a wind-induced shear stress  $\tau_w$  at the surface. The subtidal longitudinal currents thus read

$$u(x,z) = \frac{gH^3\beta}{48\rho_0 A_v} \frac{\partial S}{\partial x} p_D + \frac{3Q_R}{2Hb} p_R + \frac{\tau_w H}{4\rho_0 A_v} p_W, \tag{1}$$

where x and z are the longitudinal and vertical coordinates, positive

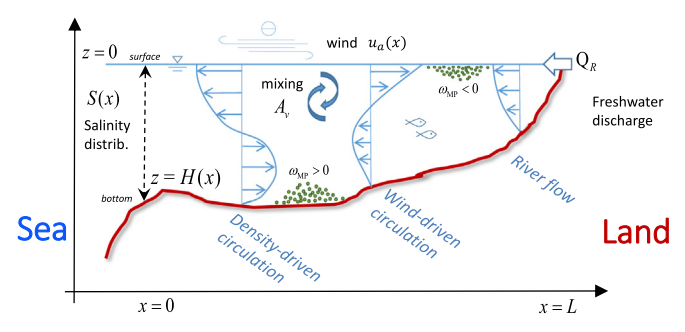


**Fig. 3.** Sketch of the lateral view of the model domain and the processes considered in the idealized model. Notice that salinity (density) distribution profile, depth, wind and width (not shown) are functions of the along-channel coordinate x. Types of MPs with negative ( $\omega_{\rm MP}>0$ ) or positive buoyancy ( $\omega_{\rm MP}<0$ ) are considered.

upstream and upwards, respectively. Their origins are the estuary mouth and the free surface, respectively. Thus, positive currents u > 0are landward while negative values indicate seaward currents. The geometry of the estuary is defined by a depth H(x) and width b(x) determined from the data sources. The polynomials  $(\xi) = 1 - 9\xi^2 - 8\xi^3$ ,  $p_R(\xi) = 1 - \xi^2$ , and  $p_W(\xi) = 1 + 4\xi + 3\xi^2$  with  $\xi = z/H$  account for the vertical structure of the density-driven, river, and wind-induced flow, respectively, at a given point x. The vertical eddy viscosity coefficient  $A_{\nu}$  is considered depth-independent. The gravitational acceleration is  $g = 9.8 \,\mathrm{ms}^{-1}$ . The parameter  $\beta = 7.6 \cdot 10^{-4} \text{psu}^{-1}$  is the haline contraction coefficient. Reference constant density values for freshwater and air are  $\rho_0 = 1000 \, kg \, m^{-3}$ and  $\rho_a = 1.22 \,\mathrm{kg} \,\mathrm{m}^{-3}$ . The shear induced by the wind is  $\tau_w = \rho_a C_{Da} u_a |\mathbf{u_{10}}|$ , with  $\mathbf{u_{10}}$  the wind velocity vector and  $u_a$  its alongchannel component. Positive (Negative) values of  $u_a$  indicate landward (seaward) winds. A standard value  $C_{Da} = 1.28 \cdot 10^{-3}$  for the air-water drag coefficient is considered.

The spatial distribution of both floating and suspended MPs in estuaries is estimated from the subtidal concentration equation. Each type of MP is assumed to have a constant terminal velocity  $\omega_{\text{MP}}$ . This value is positive if the MPs sink, and negative for floating MPs. The vertical distribution of subtidal MPs concentration is obtained imposing that the vertical flux of MPs is balanced by turbulent diffusion. This reads,

$$c(x,z) = c_b(x) \exp(-\omega_{\text{MP}}(z + H(x))/K_v), \tag{2}$$

where  $c_b(x)$  is the MPs concentration at the bottom, which is determined first assuming that the estuary is at equilibrium conditions at each cross-section x of the estuary, i.e.,  $\int_{-H}^0 \left(u\,b\,c\,-\,b\,K_h\frac{\partial c}{\partial x}\right)dz=0$  (net transport vanishes). The equilibrium distribution of MPs is found using the constraint that the total mass of MP in the domain is conserved. This yields an implicit solution for  $A(x)\exp(F(x,c_b(x)))$  that is solved iteratively (Talke et al., 2009a, 2009b).

#### 2.3.2. Design of experiments

Two series of modelling experiments were designed to explain the observed distribution patterns of MPs in the Ría de Vigo and evaluate the relative importance of river discharge, wind-driven, and density-

driven circulation.

A first series of experiments was carried out to verify the ability of the idealized model to simulate as close as possible the main features of the 2D-vertical circulation and salinity field in the Ría de Vigo (Gago et al., 2011). For the model verification in the Ría, an intrusion event of the plume of the River Miño on 01/22/10 was chosen for having recent and complete circulation data, as were reported by Des et al. (2019). Intrusion of the Miño River plume is characterized by higher surface salinity values inside the Ría than at the mouth. This typically occurs when moderate to high discharges occur and northward winds blows over the shelf (e.g. Sousa et al., 2014). The vertical eddy viscosity coefficient  $A_{\nu}$  was fitted to mimic the observations. All the details on the model verification are provided in the Supplement (Appendix A).

Once the model was verified and  $A_{\nu}$  determined, the second series of experiments, whose results are presented in section 3.2, was designed to study the response of the Ría de Vigo during upwelling and downwelling conditions. The modelled distribution pattern of MPs was examined and the relative importance of the freshwater discharge, the wind-driven and the density-driven circulation were quantified. Modelled distributions of MPs were compared with the observed distribution in the Ría during those conditions. This allowed for a better understanding of the basic mechanisms that control the distribution of MPs in the Ría de Vigo. For both upwelling and downwelling conditions, realistic along-estuary salinity profiles and net freshwater discharges from Oitaven and Vedugo were set according to Gilcoto et al. (2007) and Des et al. (2019) (expressions in Table 1). Following Souto et al. (2003), wind velocity was chosen to linearly decrease from the mouth to Rande Strait. Only the along-estuary component of the wind velocity vector, which is the most significant, was considered. Local winds generally blow along the axis of the Ría because of the particular orography (López et al., 2001). Experiments to test the sensitivity of the MPs distribution patterns to uniform winds and mean salinity gradients were performed for both upwelling and downwelling conditions, as well as for MPs with positive and negative buoyancy. Wind velocities  $|u_a|$  that ranged from 5 ms<sup>-1</sup> to 15 ms<sup>-1</sup> and (scaled) mean salinity gradients  $-L\partial S/\partial x$  from 0.2 psu to 3 psu were considered. Further cases with  $Q_R = 5 \text{ m}^3 \text{s}^{-1}$ ,  $50 \text{ m}^3 \text{s}^{-1}$  and an additional, unrealistic case with  $500 \,\mathrm{m}^3 \mathrm{s}^{-1}$  were simulated to test the sensitivity of the trapping conditions to the freshwater discharges during upwelling. Pellets, fibres and fragments (e.g. fishing cuts) in the Ría de Vigo were the types of MPs considered. Effective MPs properties are indicated in Table 2. For all cases, vertical exchange coefficients were set with the values shown in Table. 1. The grid of the model is  $300 \times 100$  cells in the alongchannel and in the vertical direction. The total concentration of MPs in the estuary was normalized to unity.

# 3. Results

# 3.1. Observations

Microplastics were found in all water samples at the surface at all stations both during upwelling and downwelling conditions (Fig. 4, upper and lower panel, respectively). During the field campaigns of March and September 2017, a total of 205 plastic items were counted

**Table 1**Forcing conditions (three upper rows) and model parameters (two lower rows) for the default upwelling and downwelling cases. Distance *x* is given in km.

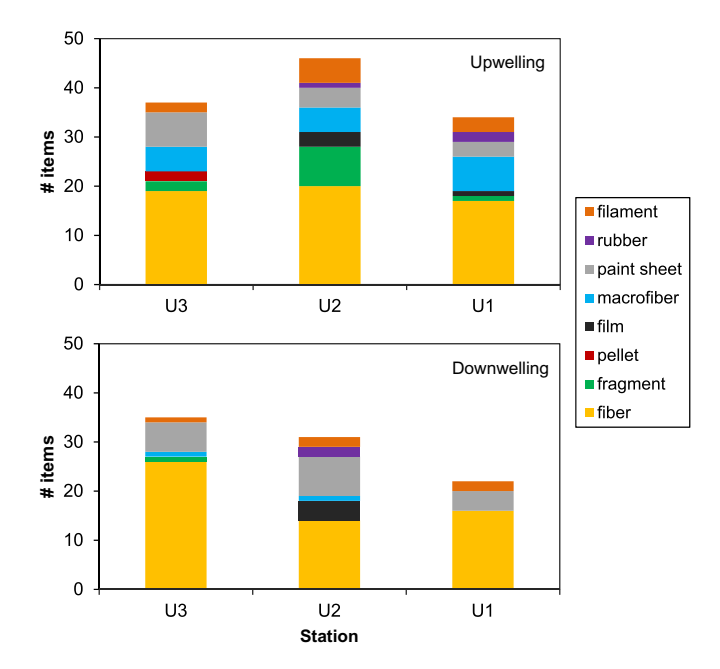
Downwelling	Upwelling
40	13
10(1-0.15x/L)	-5(1-0.15x/L)
$\frac{34.5}{2}\left(1-\tanh\left(\frac{x-25}{7}\right)\right)$	$\frac{35.8}{2}\left(1-\tanh\left(\frac{x-25}{5}\right)\right)$
0.0045	0.0045
0.0045	0.0045
	40 $10(1 - 0.15x/L)$ $\frac{34.5}{2} \left( 1 - \tanh\left(\frac{x - 25}{7}\right) \right)$ $0.0045$

Table 2

Effective plastic properties as inputs of the idealized model: type, terminal velocity  $\omega_{\text{MP}}$ , plastic density  $\rho_p$ , and radius  $R_p$ , which is estimated from waterplastic density difference and the Stokes' law, i.e.,  $\omega_{\text{MP}} = 2(\rho - \rho_p)R_p^2g/(9\eta)$ , with  $\eta = 9 \cdot 10^{-2} \text{kgs m}^{-1}$  the viscosity of water.

Туре	$\omega_{\mathrm{MP}}~(\mathrm{ms}^{-1})$	Plastic density $\rho_p  (\text{kg m}^{-3})$	Radius $R_p$ (m)
Pellet Fishing line cuts Fibres	$\pm 0.02$ $\pm 0.0067^{b}$ $\pm 1.31 \cdot 10^{-7c}$	700 - 1100 <sup>a</sup> 1135 <sup>c</sup> -	1 - 4·10 <sup>-4</sup> 0.075 <sup>b</sup>

- a Ballent et al. (2013).
- <sup>b</sup> Khatmullina and Isachenko (2017).
- c Wegner et al. (2012).

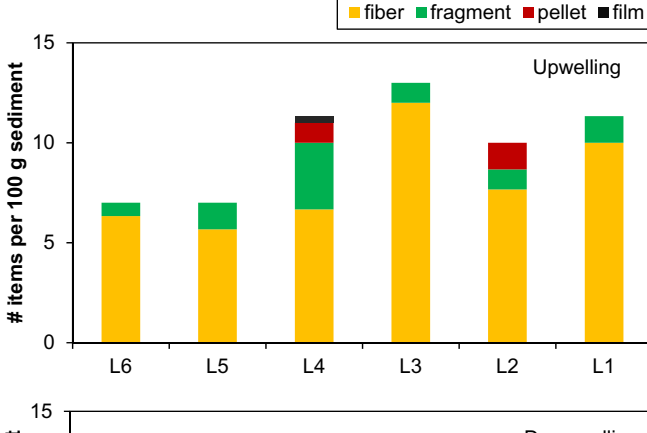


**Fig. 4.** Number of MP items sampled in the surface water stations U1-U3 shown in Fig. 1, during upwelling conditions (upper panel) and downwelling conditions (lower panel).

near the surface. The most predominant shape was fibres (56%), followed by paint sheets (15%), filaments (7%) and fragments (6%). Fibres and paint sheets account for over 70% of the plastic collected in the water surface. The rest of shapes were present in minor proportion: films (4%), rubbers (2%) and pellets (1%). The percentage of macrofibers was 9% more abundant in March 2017.

Overall, more MP items were found at all stations during spring upwelling conditions (U1 (34 items), U2 (46) and U3 (37)) than during autumn downwelling conditions (U1 (22), U2 (31) and U3 (35)) (Fig. 4, upper and lower panels, respectively). During spring upwelling conditions, an average concentration of 0.64  $\pm$  0.10 MPs m $^{-3}$  (mean  $\pm$  std) was measured in the estuary, i.e., considering all stations. During downwelling conditions, 0.48  $\pm$  0.11 MPs m $^{-3}$  were observed. Regarding the analysis by stations, U2 was slightly more polluted than U1 and U3, with average concentration values of 0.63  $\pm$  0.17 MPs m $^{-3}$ . The next more polluted stations were U3, which exhibited a MP concentration of 0.59  $\pm$  0.02 MPs m $^{-3}$  and U1, with 0.46  $\pm$  0.14 MPs m $^{-3}$ .

Regarding the color, which might give clues on the plastic origin, 44% of the samples were blue, followed by black and transparent in the same numbers (14%, respectively) and red (12%). Other colours were found in lesser proportions: green (6%), white (4%) and others like pink, purple and orange in (6%). The dominant colours of paint sheet were red and green. By contrary fibres were mostly blue and black. Filaments were transparent and pellets white.



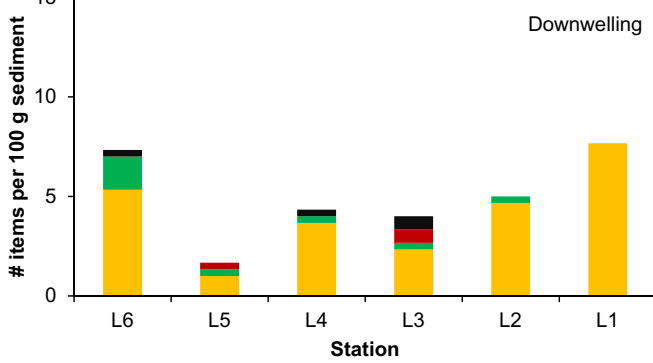


Fig. 5. Concentration of MPs, expressed as the number of particles per  $100\,g$  dry sediment, found in the bottom of the estuary at the locations L1-L6 (Fig. 1). The upper panel shows the observations made in spring (upwelling conditions), while the lower panel shows those made in autumn (downwelling conditions). Both figures are in the same scale for making possible a direct comparison.

The mean size of plastics found in seawater in Ría de Vigo was  $3.54\pm4.78\,\mathrm{mm}$  considering all stations. The most observed range is  $2-5\,\mathrm{mm}$  (38%), followed by 1 to  $2\,\mathrm{mm}$  (21%), 1 to  $0.5\,\mathrm{mm}$  (13%) and 0.5 to  $0.3\,\mathrm{mm}$  (4%). The 24% of the plastics identified were larger than  $5\,\mathrm{mm}$ .

The results of the sampling campaign at the bottom of the Ría de Vigo are shown in Fig. 5. A total of 280 MPs were observed in the bottom samples. The upper (lower) panel shows the concentration of MPs found in upwelling (downwelling) conditions. Overall, the largest observed fraction of MPs corresponded to fibres (yellow bars), which, given their shape and small size, were distributed throughout the estuary during both seasons. The next most abundant fraction was that of fragments (green bars). According to the observations, pellets (red) and films (black) were present in a smaller fraction. Comparing the observations under upwelling (upper panel) and downwelling (lower panel) conditions, it can be noticed that the amount of MPs (of any type) was larger in upwelling than in downwelling conditions, except at L6 station (mouth). Regarding the different types, fibres seemed to concentrate more in the upstream stations under upwelling conditions, while concentrations under downwelling conditions were lower in the inner part of the estuary that at the mouth. Under upwelling conditions, fragments were more efficiently trapped inside the estuary, with the highest concentrations being observed at station L4. On the contrary, downwelling conditions resulted in an overall displacement downstream of the distribution of fragments, which reaches the highest concentrations beyond the mouth (station L6). Pellet and film showed similar behavior. While these materials were trapped inside the estuary during the upwelling season (maxima at stations L2 and L4), their distribution was displaced downstream under downwelling conditions (maxima at stations L3 and L5).

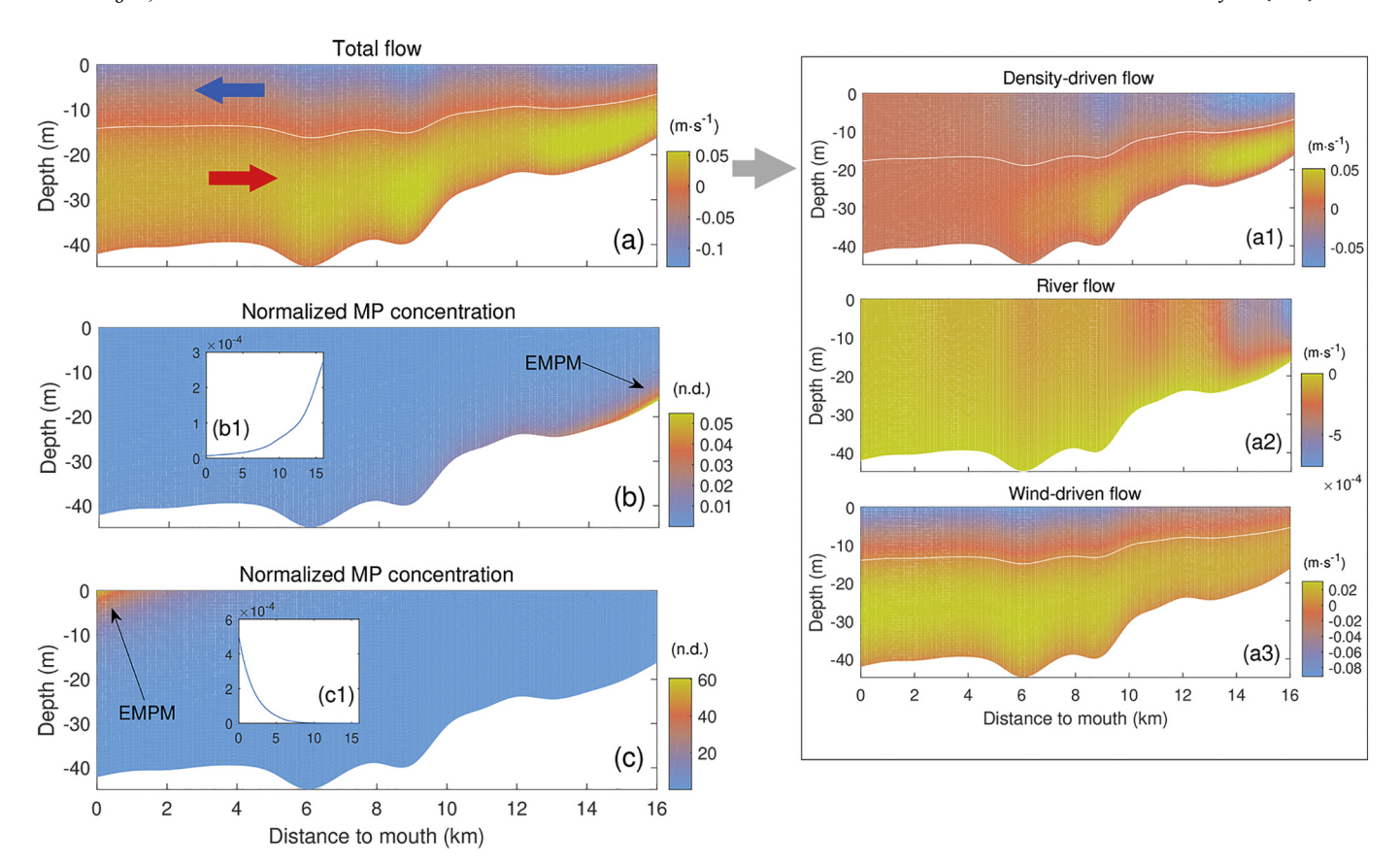


Fig. 6. Color plots for a typical configuration during upwelling conditions. Forcing parameters were set as indicated in Table 1 and type of MP was fishing cuts. Total circulation (panel a) is comprised by the superposition of the density-driven flow (a1), river flow (a2) and the wind-induced flow (a3). Panel b shows along-channel vertical profiles of normalized concentration for sinking fishing cuts. The inset b1 shows the concentration of sinking cuts at the bottom. Panel c and inset c1 show the same as panel b and inset b1 but for floating fishing cuts. Black arrows point to the estuarine MP maxima.

# 3.2. Model

# 3.2.1. Distribution of MPs during upwelling

Fig. 6 shows the net circulation (panel a) and fishing cuts distribution patterns (panels b and c) in the Ría de Vigo for typical upwelling conditions. The estuarine circulation is the result of the superposition of the density-driven flow (panel a1), river flow (a2) and wind-induced flow (a3). In these conditions, the circulation of the Ría is characterized by a vertically-sheared flow in two layers: seaward flow near the surface and landward flow near the bottom (panel a). Both wind and density gradients favour a two-layered circulation (panels a1 and a3). The river flow contribution to the residual circulation is unidirectional in the water column towards the mouth (panel a2). River flow contribution is negligible even near the head where the water depths are shallower. The mechanisms that most significantly contribute to the net circulation are the wind-driven and the density-driven circulation, which are of the same order of magnitude. The wind-induced currents are larger in a thin layer of 3-5 m below the surface.

Regarding the distribution of MPs (Fig. 6, panel b), fishing cuts with negative buoyancy are concentrated close to the bottom in the inner part of the estuary. Cuts are present at the bottom at all cross-sections, although mainly trapped near the head at the Rande Strait (more clearly seen in inset b1). The net seaward circulation near the surface induced by (mostly) wind and density gradient contributes to flushing out the floating cuts towards the mouth (panel c and inset c1). Turbulence is apparently not strong enough to diffuse the fishing cuts throughout the water column.

To test the sensibility of the EMPM to the river discharge, Fig. 7 shows the distribution of MPs at the bottom for different values of  $Q_R$  under upwelling conditions. For normal values of  $Q_R$ , viz.  $Q_R = 5 \, \mathrm{m}^3 \mathrm{s}^{-1}$ 

and 50 m<sup>2</sup>s<sup>-1</sup>, the EMPM is located at the estuary head,  $x=16\,\mathrm{km}$ , (red and blue curves). Even extreme freshwater discharges of  $Q_R=500\,\mathrm{m}^2\mathrm{s}^{-1}$  (yellow curve) move off the EMPM only to  $x\approx14\,\mathrm{km}$ . A similar behaviour is observed for other types of MPs with negative buoyancy for normal discharges. Insets a1 and a2 of Fig. 7 show the sensibility results of their EMPM to wind velocity and mean salinity gradients. The results indicate that the EMPM is always located at the inner part of the Ría, where pellets and cuts are more easily trapped than fibres. In the particular case of fibres, only with very weak winds and small density gradients, high discharge events could flush the MPs out of the Ría (panel a2).

#### 3.2.2. Distribution of MPs during downwelling

Fig. 8 shows the same information as Fig. 6, but for the downwelling case. The innermost part of the Ría is characterized by a stable twolayered circulation with seaward flow near the surface and landward compensating flow near the bottom, as the classical gravitational circulation. Near the Rande Strait the density gradient is larger than in other parts of the Ría and the density-driven and river flows dominate the net circulation (panels a1 and a2). In the lower part of the Ría, the wind-driven circulation takes over the control of the net flow (magnitude  $\sim 0.3 \,\mathrm{m\,s^{-1}}$ ), thereby favouring the onset of a reversed twolayered circulation with inflows near the surface and outflows near the bottom. The wind-driven circulation is characterized by a thin surface layer with strong landward flow and a thick lower layer with weaker seaward flow (panel a3). In that part of the Ría, the density-driven circulation is weaker ( $\sim -0.1 \, \text{ms}^{-1}$ ) and opposes to the wind-driven flow (panel a1). In middle part of the Ría, a more complex circulation in three layers arises. Inflow occurs near the surface and near the bottom, whereas in the middle of the water column, seaward flow is obtained.

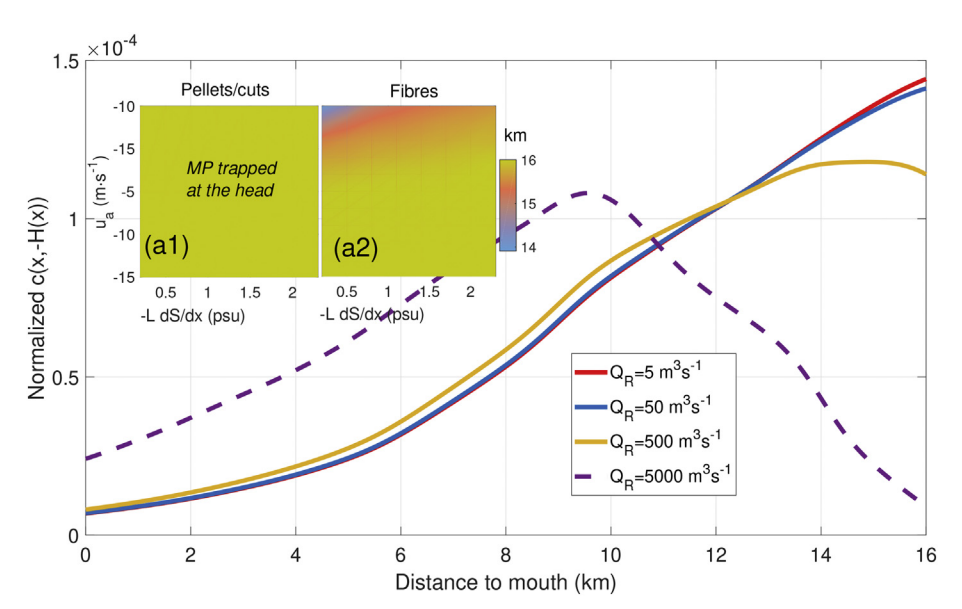


Fig. 7. Along-channel normalized concentration of sinking fishing cuts ( $\omega_{\rm MP}=0.0067~{\rm m\,s}^{-1}$ ) at the bottom during upwelling conditions for different freshwater discharge values (see legend). Insets show as color plots the location of the estuarine MP maximum at the bottom for other types of sinking MP, viz., pellets and cuts (a1) and fibres (a2), for different along-channel wind velocities ( $u_a < 0$ ) and (scaled) salinity gradients during upwelling conditions. Other parameters were set as in Table 1.

The transitions from two- to three-layered circulation occur at approximately  $x=6\,\mathrm{km}$  and  $x=13\,\mathrm{km}$ .

Regarding the distribution of sinking MPs (panel b), fishing cuts are concentrated in a thin layer close to the bottom. A significant fraction of MPs are trapped near the head due to the gravitational circulation. However, there is also a significant seaward displacement of MPs due to the wind-driven flow near the bottom. This is revealed by the secondary maximum near the mouth (inset b1). For sinking cuts (panel c and more

clearly in inset c1), the EMPM approximately coincides with the convergence of flow near the surface, as shown by the upper white line in panel a. Consequently, the location of the EMPM appears to be again mainly controlled by the competition between density-driven and wind-driven flow. To further explore the MPs distribution during downwelling events, Fig. 9 shows the sensitivity of the EMPM to different uniform along-channel wind velocities,  $u_a$ , and mean scaled salinity gradients,  $-L\partial S/\partial x$ . Upper row of panels in Fig. 9 shows the trapping

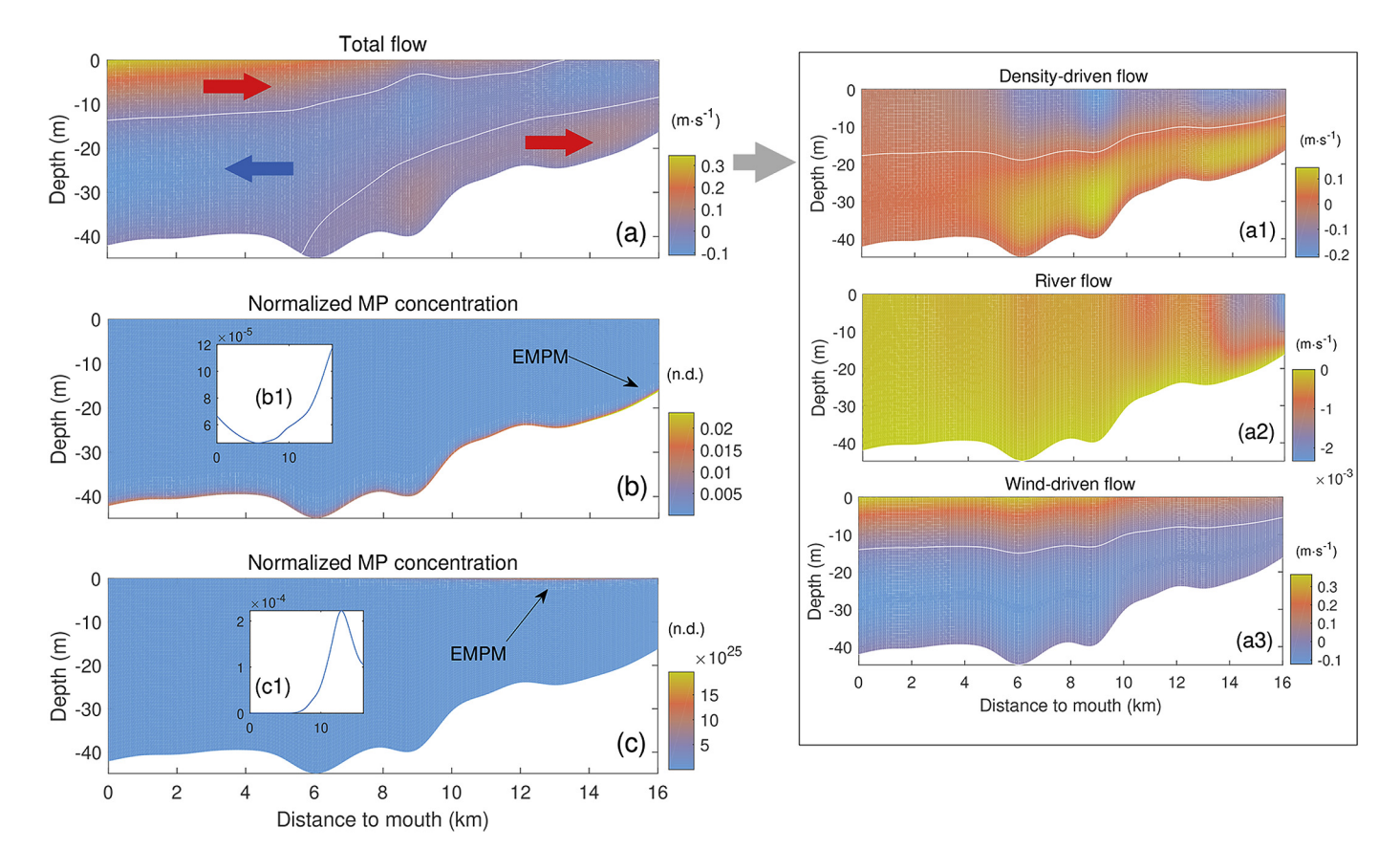
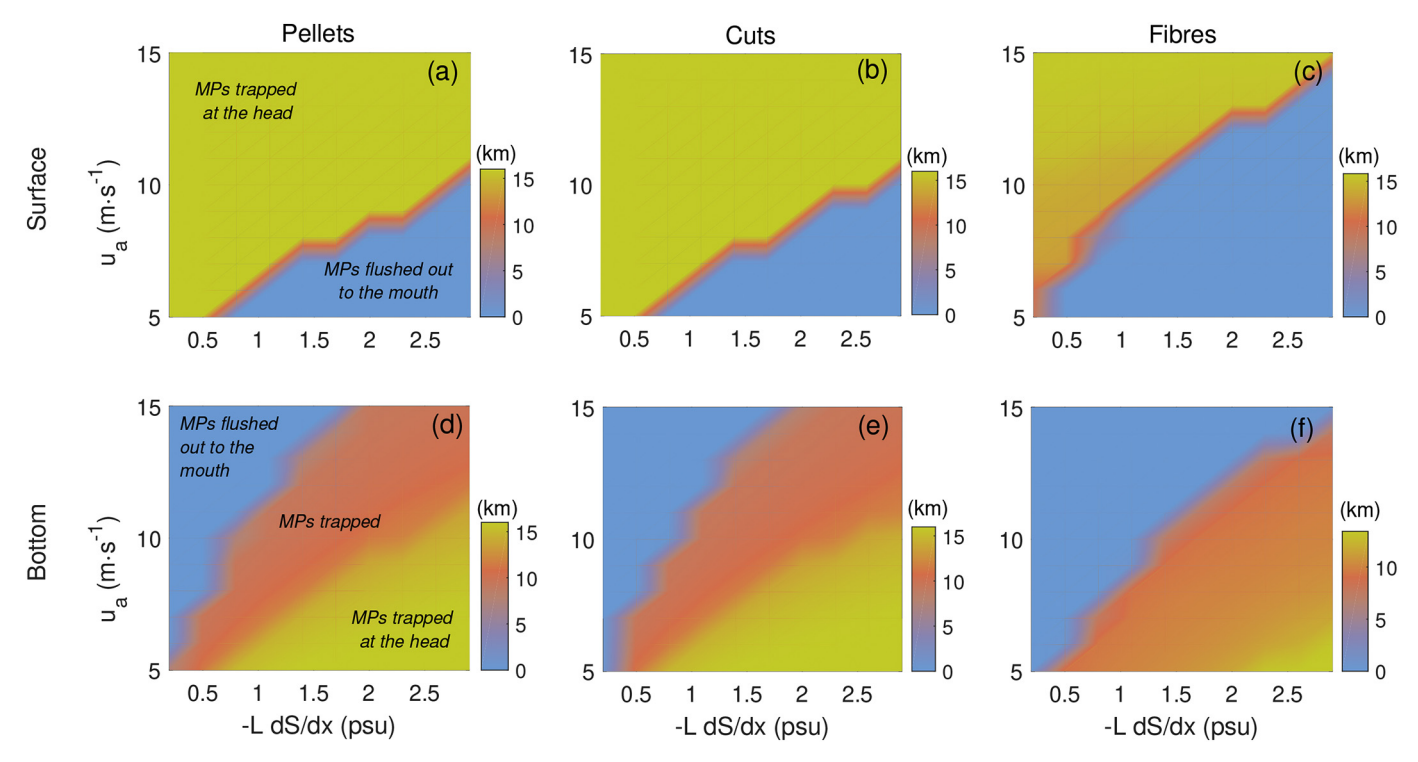


Fig. 8. Color plots for a typical configuration during downwelling conditions. Forcing parameters were set as indicated in Table 1 and MP type was fishing cuts. Total circulation (panel a) is comprised by the superposition of the density-driven flow (a1), river flow (a2) and the wind-induced flow (a3). White lines indicate zero-flow isolines. Panel b shows along-channel vertical profiles of scaled MP concentration for sinking cuts. The inset shows the concentration of sinking cuts at the bottom. Panel c and inset c1 show the same as panel b and inset b1 but for floating fishing cuts. Black arrows point to the estuarine MP maxima.



**Fig. 9.** Location of the EMPM (km) for pellets (left column of panels), fishing cuts (central column) and fibres (right column) at the surface (upper row) and at the bottom (lower row) during downwelling for different uniform along-channel wind velocities  $u_a < 0$  and (scaled) salinity gradient  $-L\partial S/\partial x$ .

location near the surface for floating pellets, cuts and fibres (panels a, b and c, respectively). In this case, the surface flow induced by downwelling-favourable winds oppose the seaward flow that is part of the gravitational circulation. Cases with relatively high wind velocities or weak density gradients and freshwater discharges yield trapping of material near the head (yellowish areas), whereas a stronger gravitational circulation (and/or weaker landward winds) favours the MPs being exported to the outer parts of the Ría and eventually to open sea. The same set of simulations was performed for negative buoyancy MPs (panels d, e and f). For instance, for cuts (panel e), the density-driven circulation is weak when the density gradients are low and thus the return flow near the bottom induced by the wind dominates the transport of MPs. The result is that the MPs are mostly flushed out the Ría (bluish areas). For low wind velocities, the density-driven circulation controls the fate of microplastics in most of the Ría, thereby trapping them mostly near the head (yellowish areas). For intermediate values of wind velocity and horizontal salinity gradients both forcings balance each other and the material is trapped at some point inside the Ría. Pellets (panel d) behave similarly. However, fibres, which have lower terminal velocity values (Table 2), are apparently more easily flushed out during downwelling events (panel f).

# 4. Discussion

Observations show that there was a persistent concentration of MPs, both at the surface and the bed, in the Ría de Vigo (Fig. 4). The highest concentration value found in surface waters in the Ría de Vigo (0.75 MPs m<sup>-3</sup>) is similar to that in the Pearl River Delta (0.7 MPs m<sup>-3</sup>) (Mai et al., 2019) and about 30 times lower than the average concentrations measured in the Changjiang Estuary (231 MPs m<sup>-3</sup>) (Xu et al., 2018). The distribution of MPs depends on the type of MP and varies in time controlled by meteorological and oceanographic conditions. Microplastic concentrations are also subject to uncertainty due to the patchiness associated with plastic pollutants. Although it is extremely difficult to identify sources of MPs with the information currently available, the presence of paint sheets plastics and fishing cuts in

the samples seems to point to fishing and port activities, which are quite intense in this area with the Port of Vigo as one of the most important fishing ports of the world. Supporting this view are the observations by Reddy et al. (2006), which found a relation between the plastic concentrations and ship-breaking activities in the Gulf of Cambay (India). Another potential source of MP fibres in the Ría is the WWTP of Vigo. More than half of the textiles used nowadays are made of (or partly made of) polymer-based plastic. Polymer-based fibres pass easily through the WWTP without being removed from the water environment (Gago et al., 2018).

During spring upwelling conditions, regardless of the particular type of MPs, more items were collected near the surface than during autumn downwelling conditions. This behaviour is successfully explained by the modelling results. The net seaward circulation near the surface induced by wind, density gradient and, to a lesser extent, freshwater discharge contributes to flushing out floating MPs (Fig. 6). The surface MPs would then be controlled by the meteorological and oceanographical conditions on the shelf, thereby increasing the probability of beaching of debris in the National Park of Cies Islands. Model results indicate that the flushing time is about 5.8 days, which is estimated from the mean outflow velocity 0.0315 ms<sup>-1</sup> at mid-estuary in the upper layer. This value is about the same order of magnitude than that reported in the literature for upwelling conditions, i.e., 5 days by Álvarez-Salgado et al. (2001) and 4.5 days by López et al. (2001). The station U1 is located near the city of Vigo, a potential significant source of MPs. However, the largest concentrations were measured at station U2, not at station U1. It is remarkable that at station U3, which is the outermost station, outside the Ría and subject to more open oceanic conditions typical of the inner shelf, the concentrations are on the same order of magnitude than within the Ría. Near the bottom, upwellings induce a landward circulation, thereby yielding the trapping of near-bed materials. Fig. 5 showed that pellets and cuts were more efficiently trapped inside the Ría than materials with lower settling velocities such as fibres. Only fibres under sustained very weak winds, small density gradients and high discharges could be flushed out of the Ría. However, this situation is rather unlikely due to the fact that river flow seems to be only

important to establish the density gradient that drives the density-driven circulation (Villacieros-Robineau et al., 2013).

Regarding the downwelling conditions, lower MPs concentrations at surface stations U1, U2 and U3 were observed than during upwelling despite the wind-induced circulation favouring the trapping of floating MPs. Stations U1 and U2 show larger concentrations of paint sheets and films than the outermost station U3 (similar values of fibres were measured at U1-U3). An unlikely hypothesis is that both the densitydriven flow and river flow have exceptionally compensated for the wind-induced flow. However, the results shown in Figs. 6 and 8 indicate that wind contributes the most to the net circulation in the Ría de Vigo. This was already pointed out by a number of authors (e.g. Barton et al., 2015). The flushing or trapping of MPs in the Ría is thus mainly controlled by the wind forcing. Another more plausible hypothesis, as suggested by the model output, is that a significant fraction of the floating debris is being advected landward further than station U1 by the wind action, remaining trapped near the Rande Strait, thereby exhibiting the system lower MPs concentrations at the lower half of the estuary (precisely where stations U1-U3 were). Model results explained the overall seaward displacement of MPs at the bottom with regard to that during upwelling (Fig. 6 and Fig. 8). Similarly to what occurs during upwelling, the wind is the most significant factor controlling the flushing of near-bed MPs during the downwelling regime, particularly in the lower part of the Ría. The flushing time is calculated to be 6.04 days (mean outflow velocity 0.0300 ms<sup>-1</sup> at mid-estuary). This value is similar to that reported by Gilcoto et al. (2007) (6 days) but below the 9.5 days estimated by López et al. (2001). In the upper part, near the head, the gravitational circulation still dominates the circulation. For intermediate values of wind velocity and density gradients, the circulation induced by these factors may balance each other and MPs could be trapped at some point inside the Ría.

Important simplifications are considered in the modelling approach and should be mentioned. This is a 2D-vertical model, therefore lateral variability, which is also relevant in the Ría de Vigo (e.g. Gilcoto et al., 2007; Barton et al., 2015), is not considered. The idealized approach assumes that MPs are passive tracers that are being transported and dispersed by the water motion. The study of passive substances in estuaries has attracted considerable attention, including in the Ría de Vigo (e.g. Gomez-Gesteira et al., 1999). This assumption allows for extending the approach devised by Talke et al. (2009b), which succeeded in explaining the main features of the circulation and the Estuarine Turbidity Maxima (ETM) in the Ems estuary, to determine concentrations of both sinking and floating MPs in the Ría de Vigo. The approach adopted in this work assumes that MPs are also in suspension, but either with a positive or negative terminal velocity  $\omega_{MP}$ . The model only differentiates substances through its terminal velocity. Different substances with similar terminal velocities are expected to produce similar modelled concentration patterns. In this regard, there are evidences that MPs converge at the same locations where other substances, such as fine sediments and microorganisms, show high concentrations (Atwood et al., 2019; Payton et al., 2020). These locations may coincide with zones of convergence of living organisms, either benthic or in suspension, such as dinoflagellates, resulting in adverse consequences for the marine organisms of the Ría and potential hazard to the ecosystem (Crespo et al., 2006).

The model also neglects density stratification and the tidal variation of flow and their effect on mixing, circulation and residual transport and trapping of MPs (e.g. Munk and Anderson, 1948; Chernetsky et al., 2010). Tidal effects are expected to be relevant near the Rande Strait, where the Ría shoals and tidal currents are stronger. The turbulent mixing, parametrized in the model by means of eddy coefficients, is assumed to be uniform in the vertical direction. Density stratification is known to affect turbulence. Differences in the eddy coefficients should be expected between upwelling and downwelling conditions (Fernández-Castro et al., 2018). In the presence of stratification the eddy coefficients used in the model are expected to be reduced below

the constant values considered in this work. The model is intended and designed to provide insights on the physical processes that control the flow and MP distribution. The model has no predictive capabilities. Complex numerical models, which are routinely applied to study hydrodynamic and transport processes, could represent a reasonable complementary approach to idealized models to study and predict MPs accumulation in estuaries. Nevertheless, the application of this type of models for plastic pollution in these environments is still in its infancy, and there are also many challenges to solve associated with their application (e.g. Martins et al., 2019; Jalón-Rojas et al., 2019).

In spite of the simplifications noted above, the model used in this work was able to reproduce the main features of the observed MP distribution, to estimate the relative influence of the different forcing factors, and to identify the trapping conditions of MPs, both at the bottom and near the surface. The model correctly captured the order of magnitude and differences between flushing times during upwelling and downwelling conditions, although these differences, with the current parametrization, are aparently not so marked. The model may be easily implemented in other estuaries and has a low computational cost. This allowed us to run a large ensemble of model simulations, considering a wide range of meteorological and oceanographic conditions. This provided important insights into the sensitivity of the EMPM to different environmental conditions and the dominant processes involved. Overall, the use of idealized models could help to identify hotspots for MPs concentration in estuaries and even provide relevant information for the implementation of the European Marine Strategy Framework Directive (e.g. Gago et al., 2016).

# 5. Conclusions

Observations of MPs made at the bed and near the water surface, and modelling results in the Ría de Vigo were presented and analyzed to quantify concentration and distribution of MPs.

Microplastics were found at all stations in surface and bottom samples both during spring upwelling and autumn downwelling seasons. The highest concentration value found in surface waters was  $0.75~{\rm MPs}~{\rm m}^{-3}$ . The largest observed fraction of MPs corresponded to fibres (over 50%) followed by plastic paint sheets, fragments and others.

During upwelling conditions, more items were collected near the surface at the outer half of the estuary compared to downwelling conditions. The net seaward circulation near the surface, jointly induced by the gravitational circulation and, most significantly, the wind-induced circulation, contributed to flushing out the floating MPs. Upwelling-favourable winds induce a landward circulation near the bottom, thereby yielding the trapping of sinking MPs inside the estuary. Modelling results indicate that this landward displacement was also favoured by the normal density-driven circulation and opposed to the river-induced circulation, the latter representing a minor contribution to the net circulation in the Ría de Vigo. Pellets, fragments and films near the bottom were trapped more efficiently and further upstream than fibres.

Downwelling conditions caused an overall landward displacement of a significant fraction of the floating debris, which remained trapped near the Rande Strait, thereby exhibiting the estuary lower MPs concentrations at the lower half of the estuary. Paint sheets and films are the type of plastics that were more easily trapped. The trapping of floating MPs during downwelling conditions was also mainly controlled by the wind forcing. The wind effect normally exceeds (and opposes) that of the density gradient, except near the Rande Strait, where the gravitational circulation takes over the control of the net flow. In the middle part of the Ría, a three-layer circulation emerges due to the competition between density-driven and wind-driven flows. Wind-induced flow is dominant near the bottom in the outer part of the estuary. This behaviour explains the observed overall seaward displacement of pellets, fragments and films near the bottom during downwelling.

#### Acknowledgements

MB acknowledges funding from the European Union's Horizon 2020 research and innovation programme under the Marie Skłodowska-Curie grant agreement N°754446 and UGR Research and Knowledge Transfer Fund – Athenea3i. MDM acknowledges support from the Spanish Ministry of Science, Innovation and Universities (project PIRATES, CTM2017-89531-R). IEO co-authors acknowledge support from BASEMAN (Ref. PCIN-2015170-CO2-02) and RADIALES (IEO-Spain) programs. Finally, the authors are indebted to the Associate Editor and three anonymous Reviewers for their comments and suggestions to improve the manuscript.

# Appendix A. Supplementary data

Supplementary data to this article can be found online at https://doi.org/10.1016/j.marchem.2020.103780.

#### References

- Álvarez-Salgado, X.A., Gago, J., Miguez, B., Pérez, F.F., 2001. Net ecosystem production of dissolved organic carbon in a coastal upwelling system: the ria de Vigo, Iberian margin of the North Atlantic. Limnol. Oceanogr. 46, 135–146. https://doi.org/10. 4319/10.2001.46.1.0135.
- Andrady, A.L., 2011. Microplastics in the marine environment. Mar. Pollut. Bull. 62, 1596–1605. https://doi.org/10.1016/j.marpolbul.2011.05.030.
- Atwood, E.C., Falcieri, F.M., Piehl, S., Bochow, M., Matthies, M., Franke, J., Carniel, S., Sclavo, M., Laforsch, C., Siegert, F., 2019. Coastal accumulation of microplastic particles emitted from the Po River, northern Italy: comparing remote sensing and hydrodynamic modelling with in situ sample collections. Mar. Pollut. Bull. 138, 561–574. https://doi.org/10.1016/j.marpolbul.2018.11.045.
- Ballent, A., Pando, S., Purser, A., Juliano, M., Thomsen, L., 2013. Modelled transport of benthic marine microplastic pollution in the Nazaré Canyon. Biogeosciences 10, 7957–7970. https://doi.org/10.5194/bg-10-7957-2013.
- Barton, E.D., Largier, J., Torres, R., Sheridan, M., Trasviña, A., Souza, A., Pazos, Y., Valle-Levinson, A., 2015. Coastal upwelling and downwelling forcing of circulation in a semi-enclosed bay: ria de Vigo. Prog. Oceanogr. 134, 173–189. https://doi.org/10.1016/j.pocean.2015.01.014.
- Chernetsky, A.S., Schuttelaars, H.M., Talke, S.A., 2010. The effect of tidal asymmetry and temporal settling lag on sediment trapping in tidal estuaries. Ocean Dyn. 60, 1219–1241. https://doi.org/10.1007/s10236-010-0329-8.
- Cole, M., Lindeque, P., Halsband, C., Galloway, T.S., 2011. Microplastics as contaminants in the marine environment: a review. Mar. Pollut. Bull. 62, 2588–2597. https://doi. org/10.1016/j.marpolbul.2011.09.025.
- Cózar, A., Echevarra, F., González-Gordillo, J.I., Irigoien, X., Úbeda, B., Hernández-León, S., Palma, Á.T., Navarro, S., Garca-de Lomas, J., Ruiz, A., et al., 2014. Plastic debris in the open ocean. Proc. Natl. Acad. Sci. U. S. A. 111, 10239–10244. https://doi.org/10.1073/pnas.1314705111.
- Crawford, C.B., Quinn, B., 2016. Microplastic Pollutants. Elsevier Limited.
- Crespo, B., Figueiras, F., Porras, P., Teixeira, I., 2006. Downwelling and dominance of autochthonous dinoflagellates in the NW Iberian margin: the example of the Ra de Vigo. Harmful Algae 5, 770–781. https://doi.org/10.1016/j.hal.2006.03.006.
- de Swart, H.E., Schuttelaars, H.M., Talke, S.A., 2009. Initial growth of phytoplankton in turbid estuaries: a simple model. Cont. Shelf Res. 29, 136–147. https://doi.org/10. 1016/j.csr.2007.09.006.
- Des, M., deCastro, M., Sousa, M., Dias, J., Gómez-Gesteira, M., 2019. Hydrodynamics of river plume intrusion into an adjacent estuary: the Minho River and Ria de Vigo. J. Mar. Syst. 189, 87–97. https://doi.org/10.1016/j.jmarsys.2018.10.003.
- Eisma, D., 2012. Suspended Matter in the Aquatic Environment. Springer Science & Business Media, Berlin Heidelberg.
- Fernández, E., Álvarez-Salgado, X.A., Beiras, R., Ovejero, A., Méndez, G., 2016.

  Coexistence of urban uses and shellfish production in an upwelling-driven, highly productive marine environment: the case of the Ra de Vigo (Galicia, Spain). Reg. Stud. Mar. Sci. 8, 362–370. https://doi.org/10.1016/j.rsma.2016.04.002.
- Fernández-Castro, B., Gilcoto, M., Naveira-Garabato, A.C., Villamaña, M., Graña, R., Mouriño-Carballido, B., 2018. Modulation of the semidiurnal cycle of turbulent dissipation by wind-driven upwelling in a coastal embayment. J. Geophys. Res. Ocean. 123, 4034–4054.
- Frias, J., Pagter, E., Nash, R., O'Connor, I., Carretero, O., Filgueiras, A., Viñas, L., Gago, J., Antunes, J., Bessa, F., Sobral, P., Goruppi, A., Tirelli, V., Pedrotti, M.L., Suaria, G., Aliani, S., Lopes, C., Raimundo, J., Caetano, M., Palazzo, L., De Lucia, G.A., Camedda, A., Muniategui, S., Grueiro, G., Fernandez, V., Andrade, J., Dris, R., Laforsch, C., Scholz-Böttcher, B.M., 2018. Standardised protocol for monitoring microplastics in sediments. In: JPI-Oceans BASEMAN project.
- Gago, J., Cabanas, J., Casas, G., Miranda, A., 2011. Thermohaline measurements in the continental shelf zone of the NW Iberian Peninsula, 1994–2006. Clim. Res. 48, 219–229. https://doi.org/10.3354/cr00943.
- Gago, J., Galgani, F., Maes, T., Thompson, R.C., 2016. Microplastics in seawater: recommendations from the marine strategy framework directive implementation process. Front. Mar. Sci. 3, 219. https://doi.org/10.3389/fmars.2016.00219.

Gago, J., Carretero, O., Filgueiras, A., Viñas, L., 2018. Synthetic microfibers in the marine environment: a review on their occurrence in seawater and sediments. Mar. Pollut. Bull. 127, 365–376. https://doi.org/10.1016/j.marpolbul.2017.11.070.

- Geyer, R., Jambeck, J.R., Law, K.L., 2017. Production, use, and fate of all plastics ever made. Sci. Adv. 3, e1700782. https://doi.org/10.1126/sciadv.1700782.
- Gilcoto, M., Pardo, P.C., Álvarez-Salgado, X.A., Pérez, F.F., 2007. Exchange fluxes between the Ra de Vigo and the shelf: a bidirectional flow forced by remote wind. J. Geophys. Res. Ocean. 112, C06001. https://doi.org/10.1029/2005JC003140.
- Gomez-Gesteira, M., Montero, P., Prego, R., Taboada, J.J., Leitao, P., Ruiz-Villarreal, M., Neves, R., Perez-Villar, V., 1999. A two-dimensional particle tracking model for pollution dispersion in a Coruña and Vigo rias (NW Spain). Oceanol. Acta 22, 167–177. https://doi.org/10.1016/S0399-1784(99)80043-7.
- Hansen, D.V., Rattray Jr., M., 1965. Gravitational circulation in straits and estuaries. J. Mar. Res. 23, 104–122.
- Hidalgo-Ruz, V., Gutow, L., Thompson, R.C., Thiel, M., 2012. Microplastics in the marine environment: a review of the methods used for identification and quantification. Environ. Sci. Technol. 46, 3060–3075. https://doi.org/10.1021/es2031505.
- Holmes, L.A., Turner, A., Thompson, R.C., 2014. Interactions between trace metals and plastic production pellets under estuarine conditions. Mar. Chem. 167, 25–32. https://doi.org/10.1016/j.marchem.2014.06.001.
- Jalón-Rojas, I., Wang, X.H., Fredj, E., 2019. A 3D numerical model to track marine plastic debris (TrackMPD): sensitivity of microplastic trajectories and fates to particle dynamical properties and physical processes. Mar. Pollut. Bull. 141, 256–272. https:// doi.org/10.1016/j.marpolbul.2019.02.052.
- Jambeck, J.R., Geyer, R., Wilcox, C., Siegler, T.R., Perryman, M., Andrady, A., Narayan, R., Law, K.L., 2015. Plastic waste inputs from land into the ocean. Science 347, 768–771. https://doi.org/10.1126/science.1260352.
- Kershaw, P.J., 2016. Marine plastic debris and microplastics-Global lessons and research to inspire action and guide policy change. In: Tech. Rep. United Nations Environment Programme (UNEP).
- Khatmullina, L., Isachenko, I., 2017. Settling velocity of microplastic particles of regular shapes. Mar. Pollut. Bull. 114, 871–880. https://doi.org/10.1016/j.marpolbul.2016. 11.024.
- Lebreton, L.M., Greer, S., Borrero, J.C., 2012. Numerical modelling of floating debris in the world's oceans. Mar. Pollut. Bull. 64, 653–661. https://doi.org/10.1016/j. marpolbul.2011.10.027.
- Lebreton, L.C., Van der Zwet, J., Damsteeg, J.W., Slat, B., Andrady, A., Reisser, J., 2017. River plastic emissions to the world's oceans. Nat. Commun. 8, 15611. https://doi.org/10.1038/ncomms15611.
- Lopes, C., Antelo, L.T., Franco-Ura, A., Botana, C., Alonso, A.A., 2013. Sustainability of port activities within the framework of the fisheries sector: port of Vigo (NW Spain). Ecol. Indic. 30, 45–51. https://doi.org/10.1016/j.ecolind.2013.01.040.
- López, S.T., Varela, R., Delhez, E., 2001. Residual circulation and thermohaline distribution of the Ra de vigo: a 3-D hydrodynamical model. Sci. Mar. 65, 277–289. https://doi.org/10.3989/scimar.2001.65s1277.
- Mai, L., You, S.N., He, H., Bao, L.J., Liu, L.Y., Zeng, E.Y., 2019. Riverine microplastic pollution in the Pearl River Delta, China: are modeled estimates accurate? Environ. Sci. Technol. 53, 11810–11817. https://doi.org/10.1021/acs.est.9b04838.
- Martins, I., Bessa, F., Gonçalves, A.M.M., Gago, J., Libralato, S., 2019. MODELPlastics workshop-modelling ocean plastic litter in a changing climate: gaps and future directions. Mar. Pollut. Bull. 146, 22–25. https://doi.org/10.1016/j.marpolbul.2019. 05.063.
- Masura, J., Baker, J., Foster, G., Arthur, C., Herring, C., 2015. Laboratory methods for the analysis of microplastics in the marine environment: Recommendations for quantifying synthetic particles in waters and sediments. In: NOAA Marine Debris Program National Oceanic and Atmospheric Administration US Department of Commerce. Technical Memorandum NOS-OR& R-48pp. 1.
- Mato, Y., Isobe, T., Takada, H., Kanehiro, H., Ohtake, C., Kaminuma, T., 2001. Plastic resin pellets as a transport medium for toxic chemicals in the marine environment. Environ. Sci. Technol. 35, 318–324. https://doi.org/10.1021/es0010498.
- Maximenko, N., Hafner, J., Niiler, P., 2012. Pathways of marine debris derived from trajectories of lagrangian drifters. Mar. Pollut. Bull. 65, 51–62. https://doi.org/10. 1016/j.marpolbul.2011.04.016.
- McClain, C.R., Chao, S.Y., Atkinson, L.P., Blanton, J.O., De Castillejo, F., 1986. Wind-driven upwelling in the vicinity of Cape Finisterre. Spain. J. Geophys. Res. Ocean. 91, 8470–8486. https://doi.org/10.1029/jc091ic07p08470.
- Munk, W., Anderson, E., 1948. Notes on a theory of the thermocline. J. Mar. Res. 7, 276–295.
- Nizzetto, L., Bussi, G., Futter, M.N., Butterfield, D., Whitehead, P.G., 2016. A theoretical assessment of microplastic transport in river catchments and their retention by soils and river sediments. Environ Sci Process Impacts 18, 1050–1059. https://doi.org/10. 1039/c6em00206d.
- Officer, C.B., 1976. Physical Oceanography of Estuaries (and Associated Coastal Waters). NY (USA) Wiley-Interscience, New York.
- Onink, V., Wichmann, D., Delandmeter, P., van Sebille, E., 2019. The role of Ekman currents, Geostrophy, and stokes drift in the accumulation of floating microplastic. J. Geophys. Res. Ocean. 124, 1474–1490. https://doi.org/10.1029/2018JC014547.
- Payton, T.G., Beckingham, B.A., Dustan, P., 2020. Microplastic exposure to zooplankton at tidal fronts in Charleston Harbor. SC USA. Estuar. Coast. Shelf Sci. 232, 106510. https://doi.org/10.1016/j.ecss.2019.106510.
- Quelle, C., Besada, V., Andrade, J.M., Gutiérrez, N., Schultze, F., Gago, J., González, J.J., 2011. Chemometric tools to evaluate the spatial distribution of trace metals in surface sediments of two Spanish ras. Talanta 87, 197–209. https://doi.org/10.1016/j. talanta 2011.09.062
- Reddy, M.S., Basha, S., Adimurthy, S., Ramachandraiah, G., 2006. Description of the small plastics fragments in marine sediments along the Alang-Sosiya ship-breaking

yard, India. Estuar. Coast. Shelf Sci. 68, 656–660. https://doi.org/10.1016/j.ecss. 2006.03.018.

- Simon-Sánchez, L., Grelaud, M., Garcia-Orellana, J., Ziveri, P., 2019. River deltas as hotspots of microplastic accumulation: the case study of the Ebro River (NW Mediterranean). Sci. Total Environ. 687, 1186–1196. https://doi.org/10.1016/j. scitotenv.2019.06.168.
- Sousa, M., Vaz, N., Alvarez, I., Gomez-Gesteira, M., Dias, J., 2014. Modeling the Minho River plume intrusion into the rias Baixas (NW Iberian Peninsula). Cont. Shelf Res. 85, 30–41. https://doi.org/10.1016/j.csr.2014.06.004.
- Souto, C., Gilcoto, M., Fariña-Busto, L., Pérez, F.F., 2003. Modeling the residual circulation of a coastal embayment affected by wind-driven upwelling: circulation of the Ra de Vigo (NW Spain). J. Geophys. Res. Ocean. 108. https://doi.org/10.1029/2002.1C001512
- Taboada, J.J., Prego, R., Ruiz-Villarreal, M., Gómez-Gesteira, M., Montero, P., Santos, A.P., Pérez-Villar, V., 1998. Evaluation of the seasonal variations in the residual circulation in the Ra of Vigo (NW Spain) by means of a 3D baroclinic model. Estuar. Coast. Shelf Sci. 47, 661–670. https://doi.org/10.1006/ecss.1998.0385.
- Talke, S.A., de Swart, H.E., de Jonge, V.N., 2009a. An idealized model and systematic process study of oxygen depletion in highly turbid estuaries. Estuar. Coasts 32, 602–620. https://doi.org/10.1007/s12237-009-9171-y.
- Talke, S.A., de Swart, H.E., Schuttelaars, H.M., 2009b. b. Feedback between residual circulations and sediment distribution in highly turbid estuaries: an analytical model. Cont. Shelf Res. 29, 119–135. https://doi.org/10.1016/j.csr.2007.09.002.
- Villacieros-Robineau, N., Herrera, J., Castro, C., Piedracoba, S., Roson, G., 2013. Hydrodynamic characterization of the bottom boundary layer in a coastal upwelling

- system (Ra de Vigo, NW Spain). Cont. Shelf Res. 68, 67–79. https://doi.org/10.1016/j.csr.2013.08.017.
- Viñas, L., Franco, M.A., González, J., 2009. Polycyclic aromatic hydrocarbon composition of sediments in the ria de Vigo (NW Spain). Arch. Environ. Contam. Toxicol. 57, 42–49. https://doi.org/10.1007/s00244-008-9230-6.
- Wegner, A., Besseling, E., Foekema, E.M., Kamermans, P., Koelmans, A.A., 2012. Effects of nanopolystyrene on the feeding behavior of the blue mussel (Mytilus edulis l.). Environ. Toxicol. Chem. 31, 2490–2497. https://doi.org/10.1002/etc.1984.
- Windsor, F.M., Durance, I., Horton, A.A., Thompson, R.C., Tyler, C.R., Ormerod, S.J., 2019. A catchment-scale perspective of plastic pollution. Glob. Chang. Biol. 25, 1207–1221. https://doi.org/10.1111/gcb.14572.
- Woodall, L.C., Gwinnett, C., Packer, M., Thompson, R.C., Robinson, L.F., Paterson, G.L., 2015. Using a forensic science approach to minimize environmental contamination and to identify microfibres in marine sediments. Mar. Pollut. Bull. 95, 40–46. https:// doi.org/10.1016/j.marpolbul.2015.04.044.
- Wright, S.L., Thompson, R.C., Galloway, T.S., 2013. The physical impacts of microplastics on marine organisms: a review. Environ. Pollut. 178, 483–492. https://doi.org/10. 1016/j.envpol.2013.02.031.
- Xiong, X., Wu, C., Elser, J.J., Mei, Z., Hao, Y., 2019. Occurrence and fate of microplastic debris in middle and lower reaches of the Yangtze River–from inland to the sea. Sci. Total Environ. 659, 66–73. https://doi.org/10.1016/j.scitotenv.2018.12.313.
- Xu, P., Peng, G., Su, L., Gao, Y., Gao, L., Li, D., 2018. Microplastic risk assessment in surface waters: a case study in the Changjiang Estuary. China. Mar. Pollut. Bull. 133, 647–654. https://doi.org/10.1016/j.marpolbul.2018.06.020.